Supersonic bullet trajectory estimation using ballistic shock wave arrivals at an acoustic sensor array

Kam W. Lo[1]

[1]Maritime Division, Defence Science and Technology Group, 13 Garden Street, Eveleigh, NSW 2015, Australia

ABSTRACT

One approach to locate the point of fire of a supersonic bullet is to first estimate the trajectory of the bullet and then trace the trajectory back to topographic or man-made obstructions on a digital map. The supersonic flight of a bullet generates a ballistic shock wave, and the trajectory of the bullet can be estimated by measuring the time delay between the shock wave arrivals at each sensor pair of an acoustic array and using an exterior ballistics model for the bullet to account for its decreasing speed with the distance travelled. In this paper, the bullet trajectory estimation problem is formulated, followed by a Cramer-Rao lower bound error analysis. A nonlinear least-squares (NLS) solution to the bullet trajectory estimation problem is then described, which assumes the ballistic constant of the bullet is known *a priori*. Any uncertainty in the ballistic constant will degrade the accuracy of the bullet trajectory estimation and subsequently the localization accuracy for the point of fire. The performance of the NLS method when the ballistic constant is exactly known and the degrading effect of an erroneous ballistic constant are evaluated using both simulated data and real data.

1. INTRODUCTION

Hostile small arms fire poses a serious threat to the military community. A capability to locate the sniper or point of fire is essential for an effective counter-sniper system. The firing of a supersonic bullet produces two acoustic impulses: the muzzle blast (MB) generated during the launch of the bullet from the rifle and the ballistic shock wave (SW) generated by the supersonic flight of the bullet (Maher 2007). The point of fire can be located using the MB arrivals, the SW arrivals, or both at an array of acoustic sensors distributed around the target of the sniper or within the protected area (Damarla, Kaplan & Whipps 2010, Duckworth, Gilbert & Barger 1997, Lindgren, Wilsson, Gustafsson & Habberstad 2010, Lo & Ferguson 2011, Lo & Ferguson 2012). As the shooting range increases, the MB arrivals become too weak and only the SW arrivals can be used. Duckworth *et al* proposed a method using only the SW arrivals to estimate the trajectory of the bullet, which can then be used to locate the sniper if digital maps are available to trace the trajectory back to topographic or man-made obstructions (Duckworth, Gilbert & Barger 1997). Specifically, this method for bullet trajectory estimation measures the time delay between the SW arrivals at each sensor pair of the array and adopts an exterior ballistics model for the supersonic bullet to account for the deceleration of the bullet along its trajectory. The method assumes that one of the two ballistic model parameters: the ballistic constant of the bullet is known *a priori* or has been correctly determined by estimating the calibre from the received shock wave waveform. However, this assumption is impractical because the ballistic constant spans a wide range of values due to a large number of bullet types that are available (Lo & Ferguson 2015), and there is not a one-to-one relationship between the ballistic constant of the bullet and its calibre (Lo & Ferguson 2016). Any uncertainty in the ballistic constant will degrade the accuracy of the bullet trajectory estimation and subsequently the accuracy of the sniper localization. This paper formulates the bullet trajectory estimation problem and presents a Cramer-Rao lower bound (CRLB) error analysis. A nonlinear least-squares (NLS) solution to the bullet trajectory estimation problem is then described, which assumes the ballistic constant of the bullet is known *a priori* or has been correctly estimated by some means. The performance of the NLS method when the ballistic constant is exactly known and the degrading effect of an erroneous ballistic constant are evaluated using both simulated data and real data recorded from a field experiment for two different types of bullets.

2. PROBLEM FORMULATION

Figure 1(a) shows the general geometrical configuration for an array of N acoustic sensors, the point of fire G, and the linear trajectory of the bullet passing through a point Q on the YZ-plane. The position vector of sensor n (denoted as S_n) is given by $\mathbf{R}_n = [X_n, Y_n, Z_n]^T$, for $1 \le n \le N$, and the position vectors of the two points G and Q are given by $\mathbf{R}_G = [X_G, Y_G, Z_G]^T$ and $\mathbf{R}_Q = [0, Y_Q, Z_Q]^T$, respectively, where the superscript T denotes vector transpose.

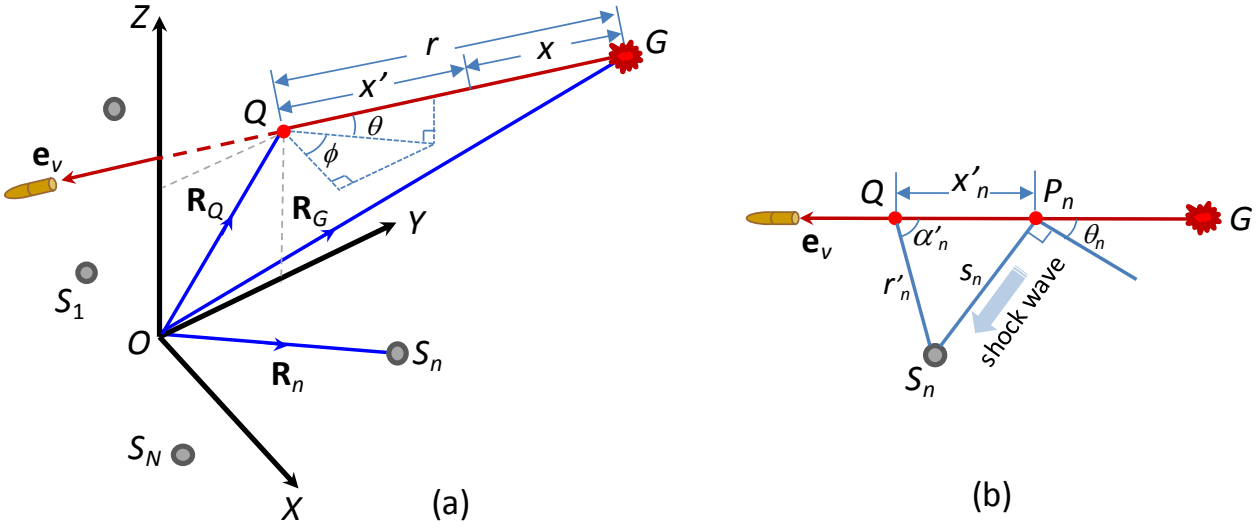

Figure 1: (a) General geometric configuration for an array of *N* acoustic sensors, the point of fire *G*, and the linear trajectory of the bullet passing through a point *Q* on the *YZ*-plane. (b) Schematic diagram showing the bullet trajectory, point of fire *G*, point *Q*, and detach point P_n of the SW arriving at sensor S_n.

The direction of travel of the bullet is described by the unit directional vector $\mathbf{e}_v = -[\cos\theta\cos\phi, \cos\theta\sin\phi, \sin\theta]^T$, where θ and ϕ are the respective elevation and azimuth angles of the point of fire *G* relative to point *Q*. The trajectory of the bullet is specified by the set of four parameters $\{\theta, \phi, Y_Q, Z_Q\}$.

2.1 Ballistic model

Let *x* denote the distance from the point of fire *G* along the bullet trajectory – see Fig. 1(a), and *c* the speed of sound in air. The (supersonic) speed of the bullet at *x* can be expressed accurately as (Lo & Ferguson 2016)

$$v(x) = (V_0^{1/2} - C_b^{-1}x)^2, \quad 0 \le x \le x_c, \tag{1}$$

where $V_0 = v(0)$ is the muzzle speed of the bullet and C_b is its ballistic constant in $(\text{m.s})^{0.5}$; $x_c = C_b(V_0^{1/2} - c^{1/2})$ is the distance beyond which the bullet speed becomes subsonic. The time required for the bullet to travel to a distance *x* from the point of fire *G* can be derived from (1) as (Lo & Ferguson 2012)

$$t(x) = C_b[v(x)^{-1/2} - V_0^{-1/2}], \quad 0 \le x \le x_c. \tag{2}$$

Let r $(< x_c)$ denote the distance from the point of fire *G* to point *Q*. The variable $x' = r - x$ then represents the displacement from point *Q* along the bullet trajectory – see Fig. 1(a); x' is positive if $r > x$ and negative otherwise. Substituting $x = r - x'$ into (1) and after some manipulation gives

$$v'(x') \equiv v(r - x') = (V_r^{1/2} + C_b^{-1}x')^2, \quad r - x_c \le x' \le r, \tag{3}$$

where $V_r \equiv v(r) = (V_0^{1/2} - C_b^{-1}r)^2$ is the speed of the bullet at point *Q*. The quantity $v'(x')$ represents the speed of the bullet at a position x' relative to point *Q*. Substituting $x = r - x'$ into (2) and after some manipulation gives

$$t'(x') \equiv t(r - x') = t(r) - C_b[V_r^{-1/2} - v'(x')^{-1/2}], \quad r - x_c \le x' \le r, \tag{4}$$

where $t(r) = C_b(V_r^{-1/2} - V_0^{-1/2})$ is the time required for the bullet to travel from the point of fire *G* to point *Q*. The

quantity $t'(x')$ represents the time required for the bullet to travel from the point of fire *G* to a position x' relative to point *Q*. When $x' > 0$, the second term in (4) is positive and represents the bullet's time of travel to point *Q* from a distance x'. When $x' < 0$, the second term in (4) is negative and its magnitude represents the bullet's time of travel to a distance $|x'|$ from point *Q*. It can be easily shown that taking the limit as $C_b \to \infty$ (equivalent to the bullet travelling at a constant speed $V_0 = V_r$) reduces (4) to $t'(x') = t(r) - x'/V_r$.

2.2 Time delay model

Figure 1(b) is a schematic diagram showing the bullet trajectory, point of fire *G*, point *Q*, sensor S_n, and detach point P_n of the SW arriving at S_n, $1 \le n \le N$. The detach point P_n is located on the trajectory at a position x'_n relative to point *Q*. If P_n lies before point *Q* as shown in Fig. 1(b), then $x'_n > 0$; if P_n lies after point *Q*, then $x'_n < 0$. The following derivations apply to both cases. The opening angle θ_n of the SW at P_n is given by

$$\theta_n = \sin^{-1}[c/v(x_n)] = \sin^{-1}[c/v'(x'_n)]. \tag{5}$$

The distance r'_n to point *Q* from sensor S_n, and the angle α'_n between the unit directional vector $\mathbf{e}_v$ and the position vector of point *Q* relative to sensor S_n are given, respectively, by

$$r'_n = ||\mathbf{R}_Q - \mathbf{R}_n||, \quad \cos\alpha'_n = \mathbf{e}_v^T(\mathbf{R}_Q - \mathbf{R}_n)/r'_n, \tag{6}$$

where $||.||$ denotes the L_2 norm of a vector. Applying the law of sines to the triangle P_nQS_n gives $r'_n/\cos\theta_n = x'_n/\cos(\theta_n - \alpha'_n)$, which can be expanded as

$$(x'_n - r'_n\cos\alpha'_n)\cos\theta_n = r'_n\sin\alpha'_n\sin\theta_n. \tag{7}$$

Squaring both sides of (7) and using (5) and (3) yields (after some manipulation) a sixth-order polynomial equation of x'_n:

$$f_n(x'_n \,|\, r'_n, \alpha'_n; V_r, C_b) \equiv \sum_{m=0}^{6} a_{nm} x'^{6-m}_n = 0, \tag{8}$$

where $a_{n0} = C_b^{-4}$, $a_{n1} = 2C_b^{-3}(-C_b^{-1}r'_n\cos\alpha'_n + 2V_r^{1/2})$, $a_{n2} = C_b^{-2}[(C_b^{-1}r'_n\cos\alpha'_n)^2 - 8C_b^{-1}V_r^{1/2}r'_n\cos\alpha'_n + 6V_r]$, (9a)

$$a_{n3} = 4C_b^{-1}V_r^{1/2}[(C_b^{-1}r'_n\cos\alpha'_n)^2 - 3C_b^{-1}V_r^{1/2}r'_n\cos\alpha'_n + V_r], \tag{9b}$$

$$a_{n4} = 6V_r(C_b^{-1}r'_n\cos\alpha'_n)^2 - 8C_b^{-1}V_r^{3/2}r'_n\cos\alpha'_n + V_r^2 - c^2, \tag{9c}$$

$$a_{n5} = -2r'_n\cos\alpha'_n(-2C_b^{-1}V_r^{3/2}r'_n\cos\alpha'_n + V_r^2 - c^2), \; a_{n6} = r'^2_n(V_r^2\cos^2\alpha'_n - c^2). \tag{9d}$$

Equation (8) shows that the position x'_n of the detach point P_n relative to point *Q* can be computed by finding the roots of the sixth-order polynomial equation (8). The relevant root is the real root that satisfies (7).

The time of arrival of the SW at sensor S_n is given by

$$\tau_n = t'(x'_n) + s_n/c, \tag{10}$$

where s_n is the distance from P_n to S_n. It can be shown from Fig. 1(b) that

$$s_n = r'_n\sin\alpha'_n/\cos\theta_n. \tag{11}$$

The time delay τ_{nm} between the SW arrivals at sensors S_n and S_m is defined as the arrival time τ_n of the SW at S_n relative to the arrival time τ_m of the SW at S_m: $\tau_{nm} = \tau_n - \tau_m$. Using (10) and (4), τ_{nm} can be expressed as

$$\tau_{nm} = C_b[v'(x'_n)^{-1/2} - v'(x'_m)^{-1/2}] + (s_n - s_m)/c\ ,\ 1 \le m,n \le N\ . \tag{12}$$

Equations (3), (5)-(9), (11) and (12) constitute a time delay model for the SW arrivals at sensors S_n and S_m. Define the bullet trajectory parameter vector $\boldsymbol{\lambda} = [\theta, \phi, Y_Q, Z_Q]^T$. This time delay model is a function of $\boldsymbol{\lambda}$, V_r and C_b, i.e., $\tau_{nm} \equiv \tau_{nm}(\boldsymbol{\lambda}, V_r, C_b)$. Given the bullet trajectory parameter vector $\boldsymbol{\lambda}$, the speed V_r of the bullet at point *Q* and its ballistic constant C_b, the time delay between the SW arrivals at S_n and S_m can be computed as follows.

1. For *k = m,n,*
    a. Compute r'_k and α'_k using (6).
    b. Find x'_k using (8), (9a)-(9d), (7), (5) and (3).
    c. Compute $v'(x'_k)$ using (3) and then s_k using (11) and (5).
2. Compute τ_{nm} using (12).

2.3 Objective

In this paper any quantity with a caret ^ overhead represents an estimate of that quantity. For example, $\hat{\tau}_{k1}$ denote the estimate of the time delay τ_{k1} between the SW arrivals at sensors S_k and S_1, for $2 \le k \le N$. In the presence of additive measurement errors, these (*N*-1) time delay estimates can be written in vector form as

$$\hat{\mathbf{b}} = \mathbf{b}(\boldsymbol{\lambda}, V_r, C_b) + \mathbf{n}\ , \tag{13}$$

where $\hat{\mathbf{b}} = [\hat{\tau}_{21}, \hat{\tau}_{31}, \ldots, \hat{\tau}_{N1}]^T$, $\mathbf{b} = [\tau_{21}, \tau_{31}, \ldots, \tau_{N1}]^T$, and $\mathbf{n} = [n_1, n_2, \ldots, n_{N-1}]^T$ are the time delay observation vector, time delay model vector, and time delay observation error vector, respectively. The objective is to estimate $\boldsymbol{\lambda}$ along with V_r, given the time delay observation vector $\hat{\mathbf{b}}$ and the ballistic constant C_b of the bullet.

In this paper, X_G is assumed to be known (e.g. an obstruction exists at X_G on the digital map). Once $\boldsymbol{\lambda}$ is estimated, the distance *r* to the point of fire from point *Q* and the *y*- and *z*-coordinates (Y_G, Z_G) of the point of fire can be determined from the equation $\mathbf{R}_G = \mathbf{R}_Q - r\mathbf{e}_v$, or

$$r = X_G / \cos\theta\cos\phi\ ,\quad Y_G = Y_Q + r\cos\theta\sin\phi\ ,\quad Z_G = Z_Q + r\sin\theta\ . \tag{14}$$

3. CRLB ERROR ANALYSIS

Assume the time delay observation error vector **n** is zero-mean, Gaussian distributed, with a covariance matrix **N**. Given the ballistic constant C_b, the CRLB on the error covariance matrix for any unbiased estimator of $\{\boldsymbol{\lambda}, V_r\}$ is given by (Lindgren, Wilsson, Gustafsson & Habberstad 2010)

$$\mathbf{Q}(\boldsymbol{\lambda}, V_r \mid C_b) = \left[\nabla\mathbf{b}^T \mathbf{N}^{-1} (\nabla\mathbf{b}^T)^T\right]^{-1}, \tag{15}$$

Where $\nabla = [\partial/\partial\theta, \partial/\partial\phi, \partial/\partial Y_Q, \partial/\partial Z_Q, \partial/\partial V_r]^T$ is the gradient operator and $\nabla\mathbf{b}^T$ is evaluated at the actual values of $\boldsymbol{\lambda}$ and V_r. The expressions for the elements of $\nabla\mathbf{b}^T$ can be derived using (12), (11), (5)-(7) and (3). Using a first-order approximation, the CRLB on the error covariance matrix for any unbiased estimator of $\{Y_G, Z_G\}$ is given by

$$\mathbf{C}(Y_G, Z_G \mid C_b) = \mathbf{H}\mathbf{Q}^{-1}(\boldsymbol{\lambda}, V_r \mid C_b)\mathbf{H}^T\ , \tag{16}$$

where $\mathbf{H}^T = [\partial/\partial\theta, \partial/\partial\phi, \partial/\partial Y_Q, \partial/\partial Z_Q, \partial/\partial V_r]^T [Y_G, Z_G]$, which can be computed using (14).

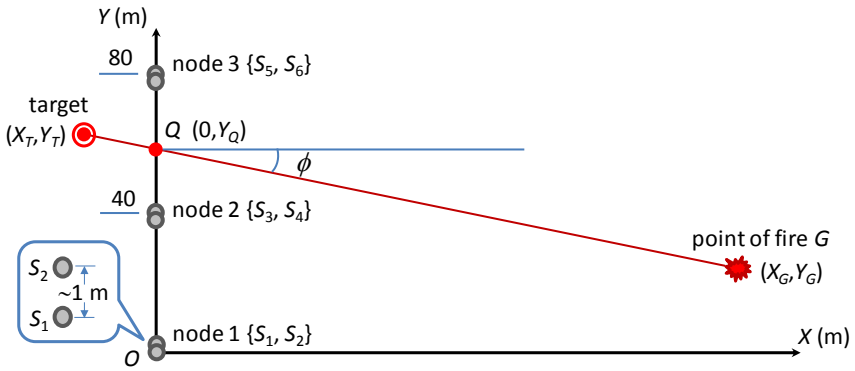

Figure 2: Geometry configuration used for CRLB analysis, simulations and field experiment.

Consider the two dimensional (2D) case as shown in Fig. 2, where the sensor array, the point of fire, and the target are located on the *XY*-plane. In this case, $\theta = Z_Q = Z_G = 0$ and $\boldsymbol{\lambda}$ reduces to $\boldsymbol{\lambda}_{2D} = [\phi, Y_Q]^T$. The array consists of three pairs of sensors (each forming an acoustic node): $\{S_1, S_2\}$, $\{S_3, S_4\}$ and $\{S_5, S_6\}$ distributed on the *Y*-axis, with S_1 located at (0, 0) and S_6 at approximately (80, 0) m. The intersensor spacing for each sensor pair (or node) is about 1 m, and the separation distance between two adjacent nodes is approximately 40 m. The array is used to estimate any bullet trajectory passing between the two outermost nodes (nodes 1 and 3).

First, consider a type 'A' 7.62 mm calibre bullet (V_o = 833.69 m/s and C_b = 90.82 (m.s)$^{0.5}$). In the first scenario, the firing position (X_G, Y_G) = (74.4, 19.6) m and the target position (X_T, Y_T) = (-44.2, 21.2) m. The CRLBs (on the error standard deviations) for $\{\hat{\phi}, \hat{Y}_Q, \hat{V}_r, \hat{Y}_G\}$ are calculated using (15) and (16) for the 2D case, and the results are shown in the last row of Table 1 (a), with the actual values of $\{\phi, Y_Q, V_r\}$ shown on top of the table. The time delay measurement error covariance matrix **N** used in (15) is derived using real data recorded from a field experiment (see Section 6). In the second scenario, the *X*-coordinate X_G of the point of fire is increased by 400 m and as a result the error covariance matrix **N** is multiplied by a realistic factor of 2.2, while other conditions remain the same as for the first scenario. The calculated CRLBs for $\{\hat{\phi}, \hat{Y}_Q, \hat{V}_r, \hat{Y}_G\}$ are shown in the last row of Table 1(b). In the third scenario, the *Y*-coordinate Y_T of the target is changed to 76.2 m while other conditions remain the same as for the second scenario. The calculated CRLBs for $\{\hat{\phi}, \hat{Y}_Q, \hat{V}_r, \hat{Y}_G\}$ are shown in the last row of Table 1(c). The above CRLB calculations are repeated for a type 'B' 5.56 mm calibre bullet (V_o = 912.37 m/s and C_b = 60.34 (m.s)$^{0.5}$), and the corresponding results for the three scenarios are shown in the last rows of Tables 2(a), (b) and (c) respectively.

4. NLS METHOD FOR BULLET TRAJECTORY ESTIMATION

The NLS method is formulated based on (13). Given an estimated (or presumed) value $\hat{C}_b$ for the ballistic constant of the bullet, the NLS estimates of $\{\boldsymbol{\lambda}, V_r\}$ are given by

$$\{\hat{\boldsymbol{\lambda}}, \hat{V}_r\} = \arg\min_{\boldsymbol{\lambda}', V_r'} [\hat{\mathbf{b}} - \mathbf{b}(\boldsymbol{\lambda}', V_r', \hat{C}_b)]^T \mathbf{N}^{-1} [\hat{\mathbf{b}} - \mathbf{b}(\boldsymbol{\lambda}', V_r', \hat{C}_b)], \tag{17}$$

where $\hat{\boldsymbol{\lambda}} = [\hat{\theta}, \hat{\phi}, \hat{Y}_Q, \hat{Z}_Q]^T$. Substituting $\{\hat{\theta}, \hat{\phi}, \hat{Y}_Q, \hat{Z}_Q\}$ into (14) gives $\{\hat{Y}_G, \hat{Z}_G\}$. Equation (17) requires the time delay measurement error covariance matrix **N**. If it is unknown, then a coarse estimate $\hat{\mathbf{N}} = \sigma^2(\mathbf{I} + \mathbf{E})$ can be used instead (where σ^2 is a constant that can be omitted; **I** is the identity matrix; **E** is the unit matrix consisting of ones), which will more or less degrade the precision of $\{\hat{\boldsymbol{\lambda}}, \hat{V}_r\}$. Any error in $\hat{C}_b$ will also induce bias errors in $\{\hat{\boldsymbol{\lambda}}, \hat{V}_r\}$. Note that the NLS estimates given by (17) are also the maximum likelihood estimates when $\hat{C}_b$ is exact and the time delay measurement error vector **n** is zero-mean, Gaussian distributed, with a covariance matrix **N**. Equation (17) can be solved iteratively using existing numerical optimization algorithms, which often require good initial estimates of

$\{\boldsymbol{\lambda}, V_r\}$ for fast convergence to the global minimum. If the acoustic array is configured as an array of acoustic nodes, each being a smaller array of sensors capable of providing estimates of the direction of arrival (DOA) of the SW at the node, then initial estimates of $\{\boldsymbol{\lambda}, V_r\}$ can be obtained using the DOA estimate of the SW at each node and the time delay estimate between the SW arrivals at each pair of nodes, with the assumption that the bullet speed is approximately constant between the detach point for each node and point *Q*. For the 2D case, the method to compute the initial estimates is similar to that described in a previous paper (Lo & Ferguson 2012).

Table 1: Simulation results (2nd to 5th rows) and CRLBs (6th row) for type 'A' 7.62 mm calibre bullet (V_o = 833.69 m/s and C_b = 90.82 (m.s)$^{0.5}$). Simulation results were obtained for different values of $\hat{C}_b$: 90.82 (actual value), 40, 200, and ∞. For each of $\{\hat{\phi}, \hat{Y}_Q, \hat{V}_r, \hat{Y}_G\}$, (1st entry, 2nd entry) = (bias error, standard deviation).

(a) First scenario: X_G = 74.45 m, Y_G = 19.64 m, Y_Q = 20.64 m, ϕ = -0.77°, V_r = 787.02 m/s

$\hat{C}_b$ (m.s)$^{0.5}$	$\hat{\phi}$ (deg)	$\hat{Y}_Q$ (m)	$\hat{V}_r$ (m/s)	$\hat{Y}_G$ (m)
90.82	**(0.01, 0.20)**	**(0.01, 0.11)**	**(-0.64, 6.99)**	**(0.02, 0.27)**
40	(0.11, 0.20)	(0.01, 0.11)	(-10.62, 7.03)	(0.14, 0.27)
200	(-0.04, 0.20)	(0.01, 0.11)	(3.78, 6.97)	(-0.04, 0.27)
∞	(-0.07, 0.20)	(0.01, 0.11)	(7.51, 6.95)	(-0.09, 0.27)
CRLB	**0.21**	**0.10**	**7.13**	**0.28**

(b) Second scenario: X_G = 474.45 m, Y_G = 19.64 m, Y_Q = 21.09 m, ϕ = -0.18°, V_r = 559.31 m/s

$\hat{C}_b$ (m.s)$^{0.5}$	$\hat{\phi}$ (deg)	$\hat{Y}_Q$ (m)	$\hat{V}_r$ (m/s)	$\hat{Y}_G$ (m)
90.82	**(0.00, 0.35)**	**(-0.03, 0.26)**	**(0.61, 5.41)**	**(-0.02, 2.85)**
40	(0.28, 0.35)	(-0.02, 0.27)	(-12.18, 5.55)	(2.31, 2.89)
200	(-0.12, 0.34)	(-0.03, 0.26)	(6.45, 5.35)	(-1.06, 2.84)
∞	(-0.23, 0.34)	(-0.03, 0.26)	(11.50, 5.30)	(-1.95, 2.83)
CRLB	**0.35**	**0.26**	**5.34**	**2.85**

(c) Third scenario: X_G = 474.45 m, Y_G = 19.64 m, Y_Q = 71.40 m, ϕ = -6.23°, V_r = 557.84 m/s

$\hat{C}_b$ (m.s)$^{0.5}$	$\hat{\phi}$ (deg)	$\hat{Y}_Q$ (m)	$\hat{V}_r$ (m/s)	$\hat{Y}_G$ (m)
90.82	**(-0.01, 0.48)**	**(-0.00, 0.10)**	**(0.17, 7.19)**	**(-0.11, 3.97)**
40	(-0.87, 0.47)	(0.21, 0.10)	(-12.14, 7.24)	(-7.08, 3.91)
200	(0.36, 0.48)	(-0.10, 0.09)	(6.06, 7.17)	(2.92, 4.01)
∞	(0.67, 0.49)	(-0.19, 0.09)	(11.37, 7.16)	(5.44, 4.06)
CRLB	**0.44**	**0.10**	**6.72**	**3.67**

5. SIMULATION RESULTS

Computer simulations were performed in MATLAB® for the same sensor configuration and scenarios considered in Section 3. Given the sensor positions (X_n, Y_n), $1 \le n \le N$, the firing position (X_G, Y_G), the target position (X_T, Y_T), and the bullet's ballistic model parameters $\{V_0, C_b\}$, the bullet trajectory parameter vector $\boldsymbol{\lambda}_{2D} = [\phi, Y_Q]^T$ and the bullet speed V_r at point *Q* were calculated using the equation $\mathbf{e}_v = (\mathbf{R}_T - \mathbf{R}_G)/||\mathbf{R}_T - \mathbf{R}_G||$, (14) and (1) . Then the time delay model vector $\mathbf{b} = [\tau_{21}, \tau_{31}, \ldots, \tau_{N1}]^T$ was computed using the procedure outlined in Section 2.2. Next, the time delay observation vector $\hat{\mathbf{b}} = [\hat{\tau}_{21}, \hat{\tau}_{31}, \ldots, \hat{\tau}_{N1}]^T$ was generated by adding a zero-mean Gaussian error vector with a covariance matrix **N** to **b**. The error covariance matrices used here were the same as those previously used for CRLB calculations. The bullet trajectory parameter vector $\boldsymbol{\lambda}_{2D}$ was estimated along with V_r using the NLS method (Eq. (17) for the 2D case), and the results were then substituted into (14) to obtain an

estimate of Y_G for the given value of X_G. The minimization in (17) was performed using the MATLAB optimization function *lsqnonlin*. The required initial estimates of $\{\boldsymbol{\lambda}_{2D}, V_r\}$ were computed as follows.

Table 2: Similar to Table 1 but for type 'B' 5.56 mm calibre bullet (V_o = 912.37 m/s and C_b = 60.34 (m.s)$^{0.5}$).

(a) First scenario: X_G = 74.45 m, Y_G = 19.64 m, Y_Q = 20.64 m, ϕ = -0.77°, V_r = 839.35 m/s

$\hat{C}_b$ (m.s)$^{0.5}$	$\hat{\phi}$ (deg)	$\hat{Y}_Q$ (m)	$\hat{V}_r$ (m/s)	$\hat{Y}_G$ (m)
60.34	**(-0.03, 0.22)**	**(0.01, 0.05)**	**(0.59, 9.47)**	**(-0.02, 0.29)**
40	(0.04, 0.23)	(0.01, 0.05)	(-4.67, 9.50)	(0.06, 0.29)
200	(-0.12, 0.22)	(0.01, 0.05)	(8.04, 9.42)	(-0.14, 0.29)
∞	(-0.16, 0.22)	(0.02, 0.05)	(11.35, 9.40)	(-0.19, 0.29)
CRLB	**0.25**	**0.05**	**9.42**	**0.32**

(b) Second scenario: X_G = 474.45 m, Y_G = 19.64 m, Y_Q = 21.09 m, ϕ = -0.18°, V_r = 499.19 m/s

$\hat{C}_b$ (m.s)$^{0.5}$	$\hat{\phi}$ (deg)	$\hat{Y}_Q$ (m)	$\hat{V}_r$ (m/s)	$\hat{Y}_G$ (m)
60.34	**(-0.01, 0.35)**	**(-0.01, 0.15)**	**(0.14, 3.82)**	**(-0.06, 2.91)**
40	(0.30, 0.36)	(-0.05, 0.15)	(-7.49, 3.89)	(2.43, 2.95)
200	(-0.46, 0.35)	(0.04, 0.15)	(11.49, 3.71)	(-3.79, 2.85)
∞	(-0.67, 0.34)	(0.06, 0.15)	(16.85, 3.66)	(-5.52, 2.84)
CRLB	**0.35**	**0.15**	**3.99**	**2.87**

(c) Third scenario: X_G = 474.45 m, Y_G = 19.64 m, Y_Q = 71.40 m, ϕ = -6.23°, V_r = 497.11 m/s

$\hat{C}_b$ (m.s)$^{0.5}$	$\hat{\phi}$ (deg)	$\hat{Y}_Q$ (m)	$\hat{V}_r$ (m/s)	$\hat{Y}_G$ (m)
60.34	**(0.02, 0.41)**	**(0.01, 0.13)**	**(0.00, 4.35)**	**(0.17, 3.43)**
40	(-0.85, 0.41)	(0.23, 0.13)	(-7.05, 4.40)	(-6.91, 3.45)
200	(1.32, 0.41)	(-0.32, 0.11)	(10.51, 4.28)	(10.72, 3.42)
∞	(1.93, 0.41)	(-0.47, 0.11)	(15.52, 4.25)	(15.64, 3.43)
CRLB	**0.41**	**0.13**	**3.83**	**3.43**

Each of the three sensor pairs $\{S_1, S_2\}$, $\{S_3, S_4\}$ and $\{S_5, S_6\}$ formed an acoustic node (see Fig. 2) that was able to provide a DOA estimate of the SW at the node. The DOA of the SW at a given node is specified by the unit directional vector pointing from the node's reference sensor S_n to the detach point P_n of the SW arriving at S_n:

$$\mathbf{e}_n = (\mathbf{R}_Q - \mathbf{R}_n - x'_n \mathbf{e}_v) / \| \mathbf{R}_Q - \mathbf{R}_n - x'_n \mathbf{e}_v \| . \tag{18}$$

Good initial estimates of $\{\boldsymbol{\lambda}_{2D}, V_r\}$ were obtained using the DOA estimates $\hat{\varphi}_5$ and $\hat{\varphi}_1$ of the SW at the respective outermost nodes $\{S_5, S_6\}$ and $\{S_1, S_2\}$, and the time delay estimate $\hat{\tau}_{51}$ between the SW arrivals at S_5 and S_1 (the respective reference sensors of these two nodes). The DOA estimates were generated by adding zero-mean, independent, Gaussian noise with a standard deviation of 0.5° to their predicted values. The initial estimates of $\{\phi, Y_Q, V_r\}$ are given by (Lo & Ferguson 2012)

$$\hat{\phi}^o = \tan^{-1}\left(\frac{\sin\hat{\varphi}_5 - \sin\hat{\varphi}_1}{\cos\hat{\varphi}_1 - \cos\hat{\varphi}_5} \right), \quad \hat{Y}_Q^o = \left| \frac{c\hat{\tau}_{51} + r_5 \sin(\hat{\phi}^o + \hat{\theta}_5 - \psi_5)}{2\cos\hat{\theta}_5 \cos\hat{\phi}^o} \right|, \quad \hat{V}_r^o = c / \sin\hat{\theta}_5 , \tag{19}$$

where $\hat{\theta}_5 = \sin^{-1}|\cos[(\hat{\varphi}_5 - \hat{\varphi}_1)/2]|$, and (r_5, ψ_5) are the polar coordinates of S_5.

For each scenario, a total of 100 simulations were carried out and the statistics of $\{\hat{\phi}, \hat{Y}_Q, \hat{V}_r, \hat{Y}_G\}$ were compiled. The bias errors and standard deviations in the estimates of these four parameters are shown in Table 1 for bullet 'A' and Table 2 for bullet 'B'. In each table, the second row corresponds to the results when the estimated value $\hat{C}_b$ in (17) equals the actual value C_b; the third to fifth rows correspond to the results when $\hat{C}_b$ equals 40, 200 and ∞ (equivalent to constant bullet speed) respectively. Both Tables 1 and 2 were obtained using the exact error covariance matrix $\mathbf{N}$ in (17). Simulations were also performed using $\hat{\mathbf{N}} = \sigma^2(\mathbf{I} + \mathbf{E})$, which resulted in slightly larger standard deviations in most cases due to the mismatch between $\hat{\mathbf{N}}$ and $\mathbf{N}$.

The following observations can be made from Tables 1 and 2. The CRLBs for $\{\hat{\phi}, \hat{Y}_Q, \hat{Y}_G\}$ increase with the firing range X_G for very small trajectory angles ϕ (cf. first and second scenarios). The CRLBs for $\{\hat{\phi}, \hat{Y}_G\}$ increase with ϕ for a given X_G (cf. second and third scenarios). When $\hat{C}_b = C_b$, all bias errors are small and all standard deviations are close to the CRLBs for each scenario. As $\hat{C}_b$ deviates from C_b, all bias errors generally increase in magnitude but there are little changes in the standard deviations for each scenario; also, the bias errors in $\{\hat{\phi}, \hat{V}_r, \hat{Y}_G\}$ obtained with $\hat{C}_b = 40\ (< C_b)$ can be larger or smaller in magnitude than those obtained with $\hat{C}_b = 200, \infty\ (\hat{C} > C_b)$ for each scenario, depending on whether the bullet is type 'A' or type 'B'. For a given $\hat{C}_b \neq C_b$, all bias errors increase in magnitude with the firing range X_G for very small trajectory angles ϕ (cf. first and second scenarios); also, the bias errors in $\{\hat{\phi}, \hat{Y}_Q, \hat{Y}_G\}$ increases in magnitude with ϕ for a given X_G (cf. second and third scenarios).

Among the results for $\hat{C}_b \neq C_b$ in Table 2(c), the root-mean-square errors (RMSEs) in $\{\hat{\phi}, \hat{Y}_Q, \hat{V}_r, \hat{Y}_G\}$ are the biggest when $\hat{C}_b = \infty$. Figure 3 shows the estimated bullet trajectories of all 100 simulations for the third scenario of bullet 'B' when (a) $\hat{C}_b$ is exact and (b) $\hat{C}_b = \infty$. Also shown in Fig. 3 are the estimated positions for the point of fire as well as the actual positions of the three sensor pairs (or nodes), the point of fire and the target.

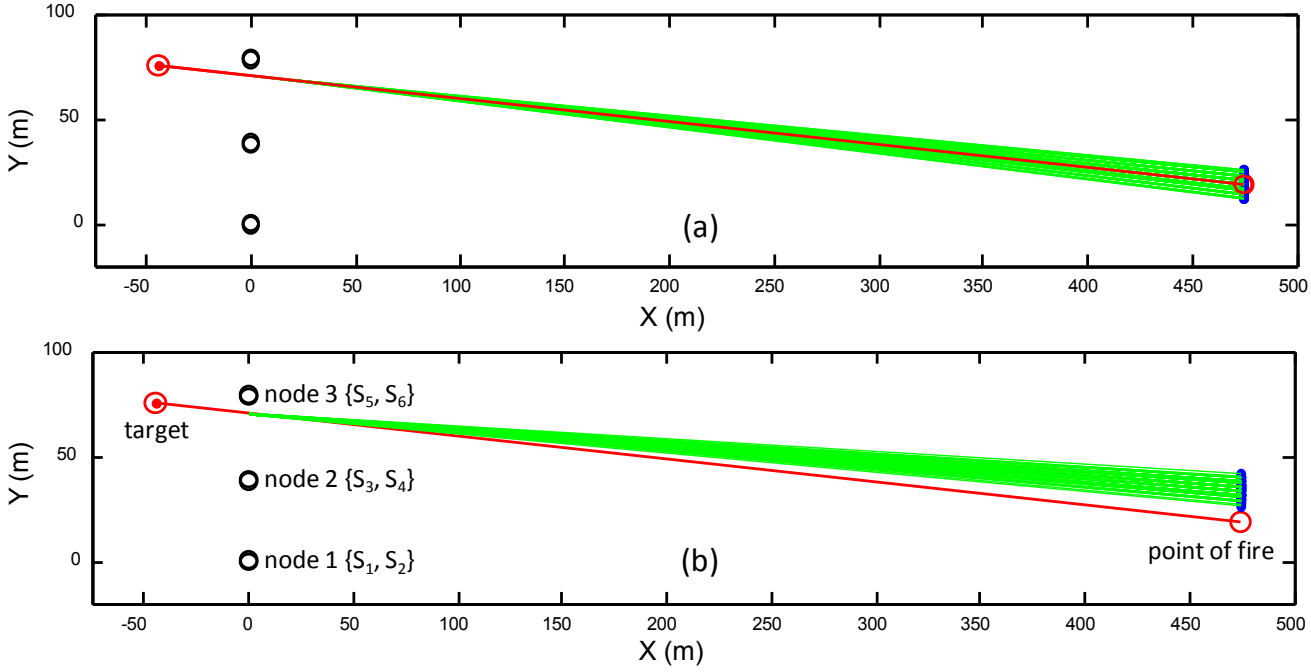

Figure 3: Estimated bullet trajectories (green lines) of all 100 simulations for the third scenario of bullet 'B' when (a) $\hat{C}_b$ is exact and (b) $\hat{C}_b = \infty$. Blue dots indicate estimated positions for the point of fire.

6. EXPERIMENTAL RESULTS

In the field experiment (Lo & Ferguson 2012), acoustic data were recorded only for a short firing range. The geometry configuration for the six sensors S_1 to S_6 (which formed three sensor pairs or acoustic nodes), the point of fire and the target was similar to Fig. 2 but they were not located exactly on the *XY*-plane. Their *X*- and *Y*-coordinates were the same as those for the first scenario considered in Sections 3 and 5. The *Z*-coordinates of the sensors ranged from 0 to 0.32 m, while those of the point of fire and the target were -1.49 m and 2.21 m respectively. However, as the separation distances between the sensors, the point of fire and the target were much larger than the differences between their *Z*-coordinates, and the horizontal miss distance was much larger than the vertical miss distance for each sensor, the assumption of a 2D geometry was approximately valid. Therefore, in the bullet trajectory estimation, the sensors, the point of fire and the target were assumed to lie on the *XY*-plane.

A total of 51 rounds of type 'A' bullet and 107 rounds of type 'B' bullet were fired. The sampling frequency of the output of each sensor was 250 kHz. For a given shot, the arrival time of the SW at each sensor was estimated using a wavelet-based edge detector (Sadler, Pham & Sadler 1998), and the results were then used to compute the time delay estimate between the SW arrivals at S_k and S_1, for $2 \le k \le 6$. The time delay error covariance matrix **N** for each bullet type was estimated using the corresponding (51 or 107) sets of time delay measurements.

The DOA φ_{2k-1} of the SW at node *k* (consisting of S_{2k-1} and S_{2k}) was estimated using the following equation

$$\hat{\varphi}_{2k-1} = \sin^{-1}(-c\hat{\tau}_{2k,2k-1}/d_k), \quad -\pi/2 < \hat{\varphi}_{2k-1} < \pi/2, \quad 1 \le k \le 3, \tag{20}$$

where $\hat{\tau}_{2k,2k-1}$ is the estimate of the time delay between the SW arrivals at S_{2k} and S_{2k-1}; d_k (~ 1 m) is the separation distance between S_{2k} and S_{2k-1}. The observed standard deviations in $\hat{\tau}_{2k,2k-1}$ and $\hat{\varphi}_{2k-1}$ are approximately 0.01 ms and 0.5° respectively, for $1 \le k \le 3$ and for both bullet types. The respective DOA estimates ($\hat{\varphi}_1$ and $\hat{\varphi}_5$) at nodes 1 and 3, and the time delay estimate ($\hat{\tau}_{51}$) between the SW arrivals at S_5 and S_1 (the respective reference sensors of nodes 3 and 1) were used in (19) to compute the required initial estimates of $\{\phi, Y_Q, V_r\}$ for the minimization in (17).

Tables 3 and 4 show the bias errors and standard deviations in the estimates of $\{\hat{\phi}, \hat{Y}_Q, \hat{V}_r, \hat{Y}_G\}$ for type 'A' and type 'B' bullets respectively. In each table, the second row corresponds to the results when the estimated value $\hat{C}_b$ in (17) is exact; the third to fifth rows correspond to the results when $\hat{C}_b$ equals 40, 200 and ∞ respectively; the last row shows the CRLBs on the error standard deviations for unbiased estimators. Tables 3 and 4 were obtained using the observed time delay error covariance matrices for bullets 'A' and 'B' in (17) respectively. Results were also obtained using $\hat{\mathbf{N}} = \sigma^2(\mathbf{I} + \mathbf{E})$, which resulted in slightly larger standard deviations. Comparing Table 3 with Table 1(a) and Table 4 with Table 2(a), the simulation results and the experimental results are in good agreement on the standard deviations, but disagree on the bias errors. When $\hat{C}_b$ equals the actual value, the bias errors from the field experiment are larger than those from the simulations. This and any other discrepancies are likely due to the measurement uncertainty in the actual values of the ballistic model parameters of the bullets, the assumption of an approximate 2D geometry, and the positional errors of the sensors, point of fire and target in the field experiment.

7. CONCLUSIONS

The performance of the NLS method for bullet trajectory estimation has been evaluated for the 2D case with a specific sensor configuration by processing simulated data (for both short and long firing ranges) and real data (for the short range only), and by comparing the error standard deviations with the CRLBs (for all scenarios). The NLS method is able to provide accurate estimates of the bullet trajectory and subsequently the position of fire (given its *X*-coordinate) for each case when the bullet's ballistic constant is exactly known. An erroneous ballistic constant has little effect on the standard deviations in the parameter estimates, but can result in large bias errors that depend on the bullet type, firing range and trajectory angle (or, in general, the positions of the target and point of fire) for the given sensor configuration. For the worst case (third scenario, bullet 'B') considered in this paper, the simulation result shows that the RMSEs in the trajectory angle and *Y*-coordinate of the point of fire are 1.38° and 11.25 m respectively when the ballistic constant (whose actual value is 60.34) is mistaken to be 200 $(\text{m.s})^{0.5}$. A possible

solution to the problem of uncertainty in the bullet's ballistic constant C_b is to extend the NLS method to estimate simultaneously both $\{\boldsymbol{\lambda}, V_r\}$ and C_b (which will require a larger number of sensors). This and the optimal placement of sensors in the protected area will be the subjects of future investigation.

Table 3: Experimental results (2nd to 5th rows) and CRLBs (6th row) for type 'A' 7.62 mm calibre bullet, X_G = 74.4 m, Y_G = 19.6m and Y_Q = 20.6 m. Experimental results were obtained for different values of $\hat{C}_b$: 90.82 (actual value), 40, 200, and ∞. For each of $\{\hat{\phi}, \hat{Y}_Q, \hat{V}_r, \hat{Y}_G\}$, (1st entry, 2nd entry) = (bias error, standard deviation).

$\hat{C}_b$ (m.s)$^{0.5}$	$\hat{\phi}$ (deg)	$\hat{Y}_Q$ (m)	$\hat{V}_r$ (m/s)	$\hat{Y}_G$ (m)
90.82	**(0.23, 0.21)**	**(0.1, 0.10)**	**(-8.48, 6.91)**	**(0.39, 0.28)**
40	(0.33, 0.21)	(0.1, 0.10)	(-18.37, 6.97)	(0.53, 0.28)
200	(0.18, 0.21)	(0.1, 0.10)	(-4.09, 6.89)	(0.34, 0.28)
∞	(0.14, 0.21)	(0.1, 0.10)	(-0.38, 6.87)	(0.28, 0.28)
CRLB	**0.21**	**0.10**	**7.13**	**0.28**

Table 4: Similar to Table 3 but for type 'B' 5.56 mm calibre bullet.

$\hat{C}_b$ (m.s)$^{0.5}$	$\hat{\phi}$ (deg)	$\hat{Y}_Q$ (m)	$\hat{V}_r$ (m/s)	$\hat{Y}_G$ (m)
60.34	**(0.14, 0.25)**	**(-0.24, 0.05)**	**(-7.51, 9.20)**	**(-0.06, 0.32)**
40	(0.21, 0.25)	(-0.25, 0.05)	(-12.78, 9.24)	(0.03, 0.32)
200	(0.04, 0.25)	(-0.24, 0.05)	(-0.02,9.15)	(-0.18, 0.31)
∞	(-0.00, 0.24)	(-0.23, 0.05)	(3.32, 9.12)	(-0.24, 0.31)
CRLB	**0.25**	**0.05**	**9.42**	**0.32**

REFERENCES

Damarla, T, Kaplan, LM, & Whipps, GT 2010, 'Sniper localization using acoustic asynchronous sensors', *IEEE Sensors Journal*, vol. 10, pp. 1469-1478.

Duckworth, GL, Gilbert, DC & Barger, JE 1997, 'Acoustic counter-sniper system', *Proceedings of SPIE*, vol. 2938, pp. 262-275.

Lindgren, D, Wilsson, O, Gustafsson, F & Habberstad, H 2010, 'Shooter localization in wireless microphone networks', *EURASIP Journal on Advances in Signal Processing*, vol. 2010, article ID 690732, pp. 1-11.

Lo, KW & Ferguson, BG 2011, 'Simultaneous classification and ranging of direct fire weapons using an asynchronous acoustic sensor network', *Proceedings of the 2011 Seventh International Conference on Intelligent Sensors, Sensor Networks and Information Processing (ISSNIP 2011)*, pp. 425-430.

Lo, KW & Ferguson, BG 2012, 'Localization of small arms fire using acoustic measurements of muzzle blast and/or ballistic shock wave arrivals', *Journal of Acoustical Society of America*, vol. 132, pp. 2997-3017.

Lo, KW & Ferguson, BG 2015, 'Acoustic ranging of small arms fire using a single sensor node collocated with the target', *Journal of Acoustical Society of America*, vol. 137, pp. EL422-EL428.

Lo, KW & Ferguson, BG 2016, 'Comparison of supersonic bullet ballistic models for accurate localization of small arms fire', *IET Radar, Sonar and Navigation*, accepted for publication. DOI: 10.1049/iet-rsn.2016.0098

Maher, RC 2007, 'Acoustical characterization of gunshots', *Proceedings of the IEEE Workshop on Signal Processing Applications for Public Security and Forensics (SAFE'07)*, pp. 109-113.

Sadler, BM, Pham, T & Sadler, LC 1998, 'Optimal and wavelet-based shock wave detection and estimation', *Journal of Acoustical Society of America,* vol. 104, Pt. 1, pp. 955-963.